Proceedings of ISINN-30, JINR, E3-2024-42, Dubna, 2024, p.117 – 127

Measurement of Fission Cross Section and Angular Distribution of Fission Fragments from Neutron-Induced Fission of ^{242}Pu in the Energy Range 0.3−500 MeV

A.M. Gagarski[1], A.S. Vorobyev[1], O.A. Shcherbakov[1], L.A. Vaishnene[1], A.M. Tiagelskaia[1], N.M. Olkhovich[1], A.L. Barabanov[2,3], T.E. Kuz'mina[4]

[1]*NRC "Kurchatov Institute", B.P. Konstantinov Petersburg Nuclear Physics Institute, 188300, Gatchina, Leningrad district, Russia*
[2]*NRC "Kurchatov Institute", 123182, Moscow, Russia*
[3] *National Research Nuclear University "MEPhI", 115409, Moscow, Russia*
[4] *V.G. Khlopin Radium Institute, 194021, St.-Petersburg, Russia*

The fission cross section and angular distribution of fission fragments from the neutron-induced fission of ^{242}Pu were measured in the energy range 1−500 MeV using the GNEIS neutron time-of-flight spectrometer and the pulsed neutron source based on the 1 GeV proton synchrocyclotron of the NRC KI - PNPI (Gatchina). A description of the original experimental setup, consisting of two MWPC counters with ^{242}Pu and ^{235}U targets, is given, as well as some basic details of the experimental data processing.

The fission cross section of ^{242}Pu is determined by the ratio method using ^{235}U as a reference. Of particular interest is the angular distribution of fission fragments in the energy range 1−500 MeV. There are currently no other experimental data in this field, despite growing interest stimulated by the development of new nuclear technologies. This measurement is a part of our investigations of neutron-induced fission of the plutonium isotopes ^{239}Pu, ^{240}Pu and ^{242}Pu at intermediate energies.

Introduction

The data on nuclear fission in intermediate energy range from a few hundred eV to 500 MeV are of prime importance for the advanced nuclear technologies such as Accelerator-Driven Systems (for nuclear power generation and nuclear transmutation). The information about angular distribution of fission fragment is also very important to verify parameters of theoretical models used for adequate fission process description in neutron energy range above 20 MeV. The systematic study of angular distributions of fission fragments are very scarce in neutron energy range above 20 MeV and are practically absent for neutron energy range above 100 MeV. Namely, for ^{242}Pu there are no such data above ~ 8 MeV. Data on the angular distributions of fission fragments are important for accurate measurements of fission cross-sections, since they should be taken into account as an efficiency correction for detectors other than 4π.

High accuracy neutron induced fission cross section data on the even-even isotopes are required to make nuclear technology safer and more efficient and to meet the upcoming needs for the future generation of nuclear power plants (GEN-IV and ADS).

The practical implementation of plans for both the creation of a closed fuel cycle based on fast nuclear reactors and the disposal of radioactive waste is impossible without reliable and accurate nuclear data. The required accuracy of the fission cross section of ^{242}Pu(n,f) is 2−5 times higher (see Table 1) than currently available [1].

Table 1. Fission cross section of ^{242}Pu: present and required uncertainties.

	Initial versus target uncertainties (%)		
Energy Range	*Present*	*SFR*	*ADMAB*
6.07 − 19.6 MeV	37	15	
2.23 − 6.07 MeV	15	5	7
1.35 − 2.23 MeV	21	5	5
0.498 − 1.35 MeV	19	4	4
183 − 498 keV	19	9	

SFR− sodium-cooled fast reactor, ADMAB− the accelerator-driven minor actinide burner reactor.

The data available on the fission cross section of ^{242}Pu are mainly limited to the neutron energies below 20 MeV. Most of this data was obtained using monoenergetic neutrons obtained in various reactions at accelerators. The available experimental data reveals a significant scatter. There are practically no experimental data for neutron energies above 20 MeV. New measurements of the fission cross section of ^{242}Pu should be made in a wide neutron energy range on neutron beams with a continuous spectrum using the TOF method.

General description of the experiment

The measurements were carried out at the 36 m flight path of the neutron TOF-spectrometer GNEIS based on the spallation neutron source at 1 GeV proton synchrocyclotron SC-1000 of the NRC KI - PNPI (Gatchina, Russia) [2, 3]. The short pulse width 10 ns of the neutron source enables to carry out TOF-measurements with the energy resolution from 0.8% (at 1 MeV) to 13% (at 200 MeV). A detailed description of the set-up can be found in our previous publications [4−12]. The main features of the present measurements are described below.

Table 2. Isotopic compositions of the targets.

	^{235}U	^{242}Pu
Isotope	Mass percentage (%)	
^{235}U	99.9920	
^{234}U	0.0020	
^{236}U	0.0040	
^{238}U	0.0020	
^{242}Pu		99.65
^{240}Pu		0.092
^{239}Pu		0.25
^{238}Pu		0.0013
^{241}Am		0.0054

The fission cross section of the nucleus under study was measured relative to the neutron induced fission of ^{235}U which is known with high accuracy (standard cross section). To ensure identical conditions for measurements of fission cross sections, namely, small and equal shape samples in wide homogeneous neutron beam, 0.1-mm-thick aluminum masks were placed on the active layers of the both targets for to separate equal circular regions with a diameter of (48.0 ± 0.1) mm on the active layers.

Targets from ^{242}Pu and ^{235}U were fabricated at the Khlopin Radium Institute (St. Petersburg) by the “painting” method on aluminum substrates 0.1 mm in thickness. The isotopic compositions of the target materials are given in Table 2. The initial shapes and sizes of the active layer were different (50×100 mm^2 for ^{235}U and Ø 82 mm for ^{242}Pu). Table 3 provides information on geometry sizes of the targets, their total masses, areal densities and homogeneity, as well as target masses and activities.

To determine the scaling factor (N_{Pu2}/N_{U5}), we made α-spectrometry of the active spots with surface barrier detector in precisely known geometry.

Table 3. Parameters of the targets.

Main isotope	^{235}U	^{243}Am
Thickness of active layer (μg/cm2)	203(11)	281(14)
Homogeneity of active layer	10%	10%
Sizes of active layer (mm)	50×100	Ø 82
Total target mass (mg)	10.15(51)	14.1(7)
Main isotope mass inside mask Ø48 mm (mg)	3.480(48)	5.35(5)
Target activity inside the mask Ø48 mm (Bq)	295	9.34×10^5
Scaling factor (N_{Pu2}/N_{U5})	1.493(25)	

A general view of the experimental setup and data acquisition system is shown in Fig. 1. The setup for measuring fission cross sections and angular distributions of fission fragments (FF) consists of two low pressure gaseous coordinate-sensitive multiwire proportional counters (MWPC, 140 × 140 mm^2). Targets are located on opposite sides of the setup. The neutron beam axis came through the geometrical centers of the target and the MWPC's electrodes being perpendicular to them.

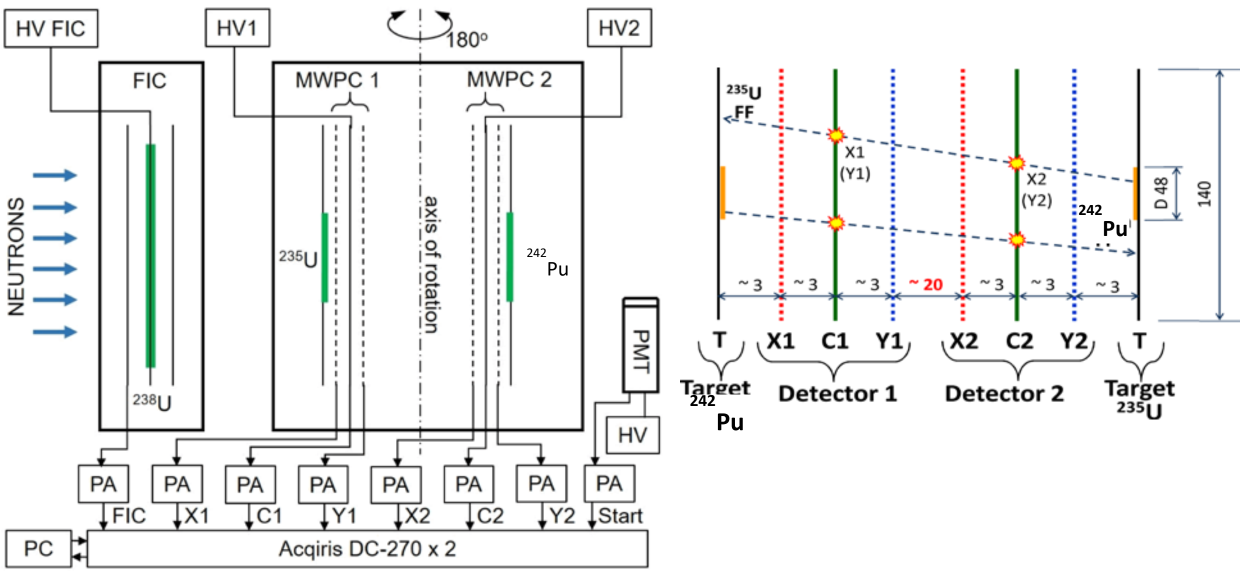

Fig. 1. Schematic view of the experimental setup and data acquisition system: left − PMT - start detector; FIC − the fission ionization chamber with ^{238}U targets (neutron flux monitor); PA – preamplifier; HV1, HV2 – high-voltage power sources; C1, C2 are the cathodes of MWPC1 and MWPC2, respectively; X1, X2 – detectors 1,2 (X axis); anodes Y1, Y2 – detectors 1,2 (Y axis); right – the internal structure of the MWPCs, the distances between electrodes and diameters are given in mm.

Data acquisition system was based on two waveform digitizers Acqiris DC-270 with sampling rate of 500 MSamples/s. This system as well as the methods of digital processing of signals from used FF detector enabled to perform measurements in a wide interval of neutron energy with a zero dead time. Herewith, almost perfect separation between fission events and products of other reactions was achieved at a practically zero FF registration threshold. To demonstrate the quality of this separation, for nuclei under study the amplitude spectra of fission fragments are shown in Fig. 2 for all events and for "useful" fission events selected by means of the procedure described in [5].

During the measurements, the fission fragments of both nuclei under study are detected simultaneously by the same MWPCs. Therefore, when processing data, it is necessary to identify a fissioning target whose fragment is detected (^{235}U or ^{242}Pu). This identification was made using the time-of-flight spectra of fission fragments presented in Fig. 3, which shows the result of measuring the time of flight of a fission fragment from the cathode of MWPC2 to the cathode of MWPC1. Two separate groups of events are clearly visible, which correspond to the fission of ^{242}Pu and ^{235}U.

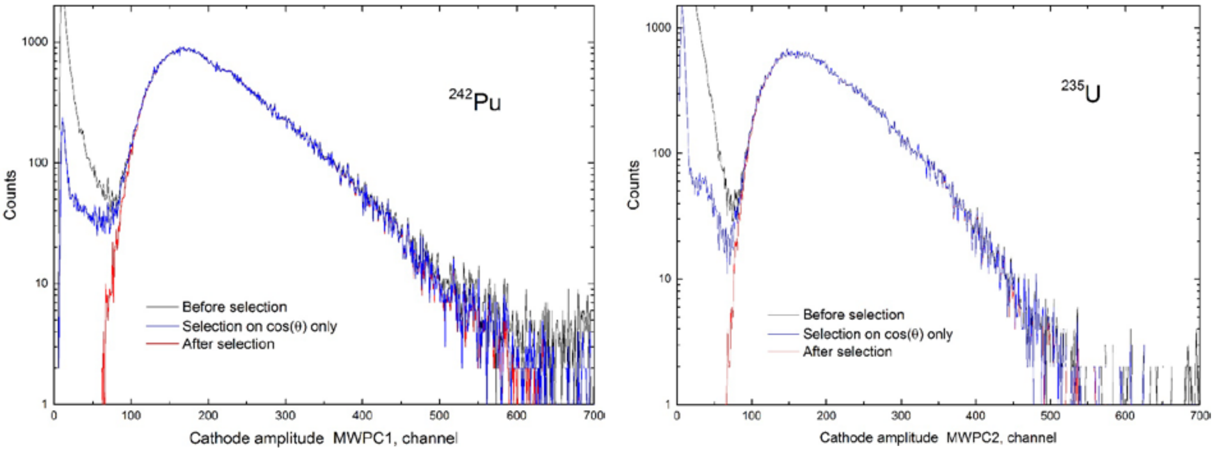

Fig. 2. The amplitude spectra of the signals from the MWPC cathode closest to the target of ^{242}Pu (left) and ^{235}U (right), respectively. A continuous line indicates the spectrum obtained after the selection of "true" events, and a dashed line – before the selection.

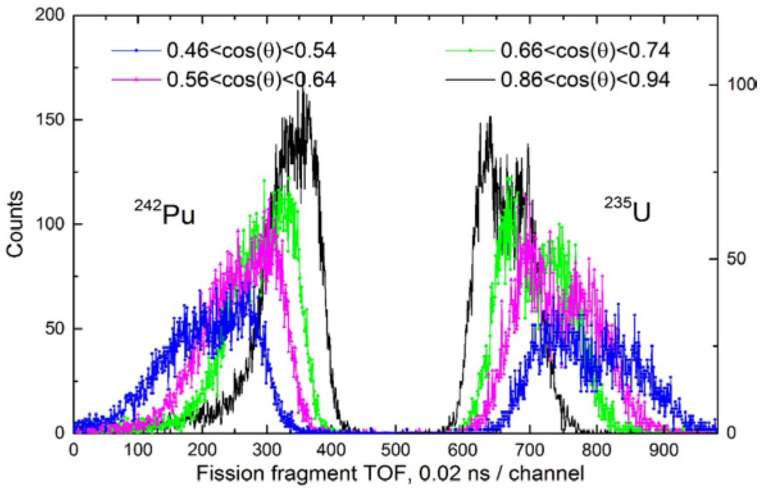

Fig. 3. Time-of-flight spectrum of fission fragments of (left part) ^{242}Pu and (right part) ^{235}U from the 500-th channel at various angles θ.

In addition to the α-decay mode, the ^{242}Pu nucleus also has a spontaneous fission decay mode with a probability 5.5×10^{-6}. This creates a non-correlated background of spontaneous fission events. The background from spontaneous fissions was 1.75±0.04 1/s. It was calculated based on the efficiency of detection of fission fragments, the spontaneous fission half-life for ^{242}Pu, and the mass of ^{242}Pu in ``masked" target precisely determined in this work. Thus, at neutron energy ~200 keV the share of spontaneous fission in the total fission fragments counts rate was ~10%, at energies ~0,3 MeV, it does not exceed 2%, and at energies ~1 MeV, it does not exceed 0.02%. The spontaneous fission background was subtracted from the time-of-flight spectra and from the measured angular distributions.

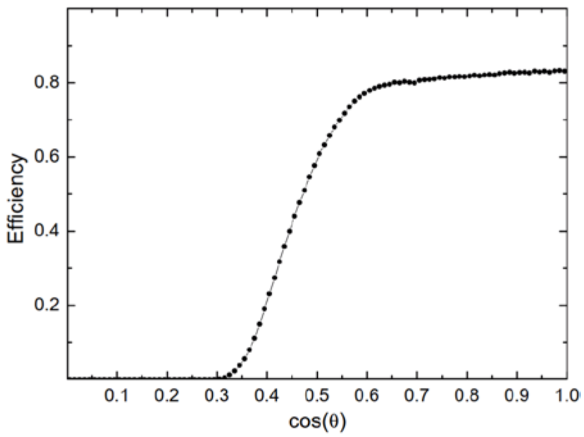

Fig. 4. The dependence of the efficiency of registration of fission fragments, ε, on the cosine of departure angle θ relative to the normal to the target plane.

The measured angular distributions for selected fission fragment events were corrected for the efficiency of fission fragment registration. This efficiency was calculated by means of the Monte-Carlo method taking into account the real geometry, design and features of the fission fragment detector the size of the active spot on the target separated by the "mask" and the spatial resolution of the MWPCs. The fission fragment detection geometrical efficiency was about 43%. The maximum fragment detection angle relative to the normal to the MWPC electrode plane was 72°. The obtained result is shown in Fig. 4.

Note that the effect of momentum transfer from the incident neutron to the fissioning system on the angular distributions in the laboratory system should be taken into account. To determine this effect, angular distributions of fission fragments in the laboratory system were measured for two setup orientations relative to the beam direction (downstream and upstream). In the first, downstream, position, the beam direction coincides with the longitudinal momentum component of the detected fission fragment. In the second, upstream, position, the beam direction is opposite to the longitudinal momentum component of the detected fission fragment.

The angular distributions of fission fragments in the center-of-mass system were deduced from the corrected cos(θ) angular distributions in the laboratory system for two set-up orientations relative to the neutron beam direction (cos(θ) bins were equal to 0.01). Then, these distributions were fitted in the range $0.35 < \cos(\theta) < 1.0$ by the sum of even Legendre polynomials up to the 4-th order and their anisotropy $W(0°)/W(90°)$ was calculated using the coefficients A_2 and A_4 (A_0=1) for the corresponding Legendre polynomials:

$$W(0°) = A_0\left[1 + \sum_{n=1}^{2} A_{2n} P_{2n}[\cos(\theta)]\right]. \quad (1)$$

$$\frac{W(0°)}{W(90°)} = \frac{1 + A_2 + A_4}{1 - A_2/2 + 3A_4/8}. \quad (2)$$

Results and discussion

As examples, the angular distributions of fission fragments for ^{242}Pu in the center of mass system for two neutron energies 0.990 MeV and 2.498 MeV data obtained in this work are shown in Fig. 5 together with the results of their fit and the other result performed earlier [13, 14]. Fig. 6 displays the preliminary data on anisotropy of fission fragments for ^{242}Pu obtained in a wide neutron energy range for the first time. The systematic error in determining anisotropy in this experiment, which is related to the finite angular resolution of the arrays with MWPC and the uncertainty in the geometry of the experiment, is about 0.5%. The systematic error associated with the approximation used for fitting is 1−1.5%.

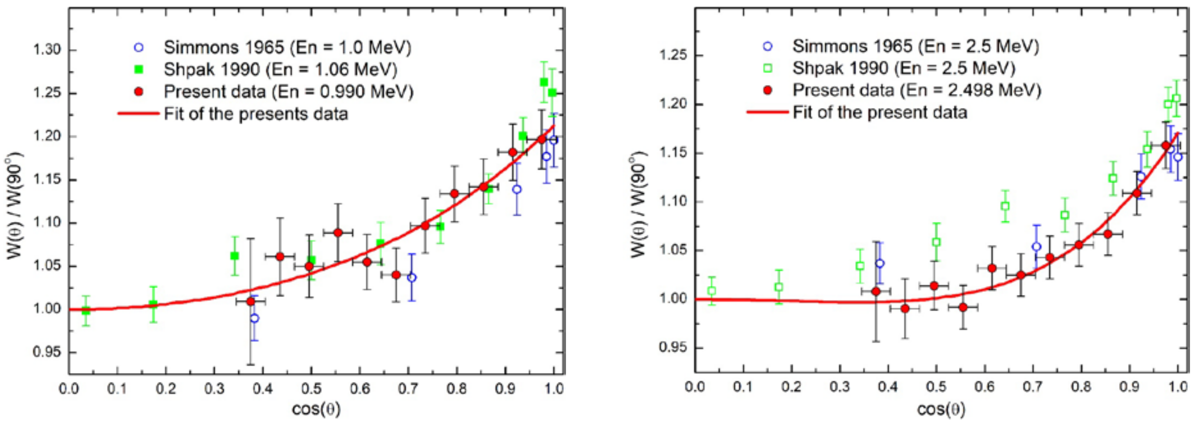

Fig. 5. Angular distributions of fission fragments for ^{242}Pu.

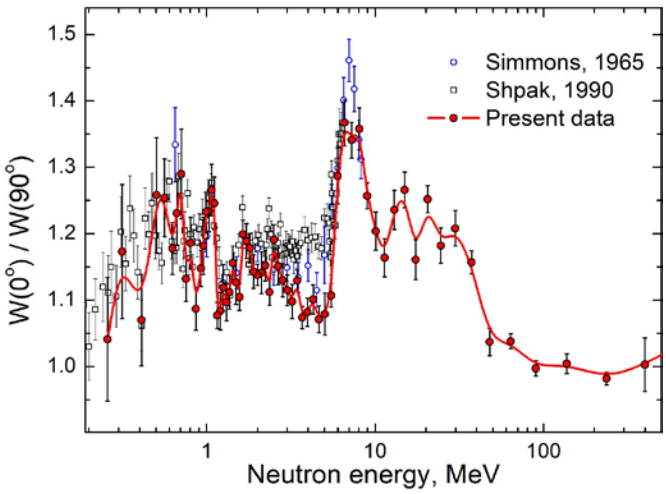

Fig. 6. Anisotropy of ^{242}Pu fission fragments in comparison with the other data [13, 14]. The indicated errors are statistical. The solid curve is shown only for visualization of experimental data.

A new stage in experimental studies of the angular distribution of fission fragments began when the GNEIS team at NRC KI - PNPI, the n_TOF collaboration at CERN and the NIFFTE collaboration at Los Alamos launched new experiments devoted to this problem almost simultaneously. The pulsed high-intensity sources of “spallation” neutrons of these facilities allow TOF-measurements of neutron-induced fission cross sections and angular distributions of fission fragments in the intermediate neutron energy range of 1−200 MeV.

Two other important features of the experimental methods used by these research groups are the use of multichannel position-sensitive fission fragment detectors of varying degrees of complexity (MWPCs, PPACs, TPC) and the use of waveform digitizers for processing detector pulses. The results of these studies are presented in Table 3. Unfortunately, the results of measurements of the anisotropy of the ^{235}U and ^{238}U fission fragments obtained by the n_TOF collaboration and published in the materials of the ND-2016 conference have not yet been presented in the EXFOR database.

Table 3. Status of experiments on angular distributions of fission fragment study.

Nucleus	GNEIS, KI-PNPI	n-TOF, CERN	NIFFTE, WNR, LANL
^{232}Th	JETP Lett.,102, 203(2015) EXFOR #41608002	Nucl. Data Sheets,119, 35 (2014) EXFOR #23209006	
^{233}U	JETP Lett.,104, 365(2016) EXFOR #41616006		
^{235}U	JETP Lett.,102, 203(2015) EXFOR #41608003 Phys. Rev. C 108, (2023) 014621, EXFOR #41757004	EPJ Web of Conf., 111 10002 (2016)	Phys. Rev. C 102, (2020) 014605, EXFOR #14660002 Phys. Rev. C 99, (2019) 064619, EXFOR #14606002
^{236}U	Phys. Rev. C 108, (2023) 014621, EXFOR #41757001		
^{238}U	JETP Lett.,102, 203(2015) EXFOR #41608004 JETP Lett.,117, 557(2023) EXFOR #41756002	EPJ Web of Conf., 111 10002 (2016)	Phys. Rev. C 102, (2020) 014605, EXFOR#14660003
^{237}Np	JETP Lett.,110, 242(2019) EXFOR #416886002		
^{239}Pu	JETP Lett.,107, 521(2018) EXFOR #41658003		
^{240}Pu	JETP Lett.,112, 323(2020) EXFOR #41737002		
^{242}Pu	Measurements completed		
^{243}Am	EPJ A, 60: 117 (2024)		
^{nat}Pb	JETP Lett.,107, 521(2018) EXFOR #41658004		
^{209}Bi	JETP Lett.,104, 365(2016) EXFOR #41616007		

The measured ratio of the neutron-induced fission cross sections of ^{242}Pu and ^{235}U is shown in Fig. 7 together with the results of other time-of-flight measurements [15–17]. Digital data were taken from the EXFOR database. It is seen that the shapes of the experimental energy dependences are very similar but there is small discrepancy in absolute value. Whereas the JENDL-5 and especially ENDF/B-VIII.0 estimates are higher than most experimental data. On the left Fig. 8 all ratio data sets available in EXFOR for comparison in the energy region below 1.2 MeV are shown. There is general agreement between experimental and evaluated data. The results of ^{242}Pu to ^{235}U cross sections ratio measurements obtained using monoenergetic neutrons produced in various reactions at accelerators are presented on the

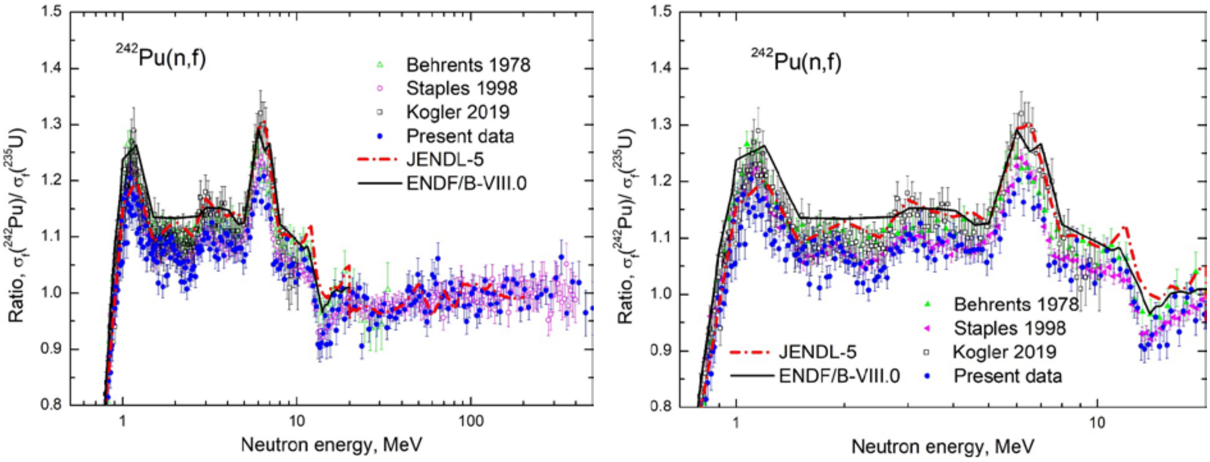

Fig. 7. Ratio of the fission cross sections of ^{242}Pu and ^{235}U.

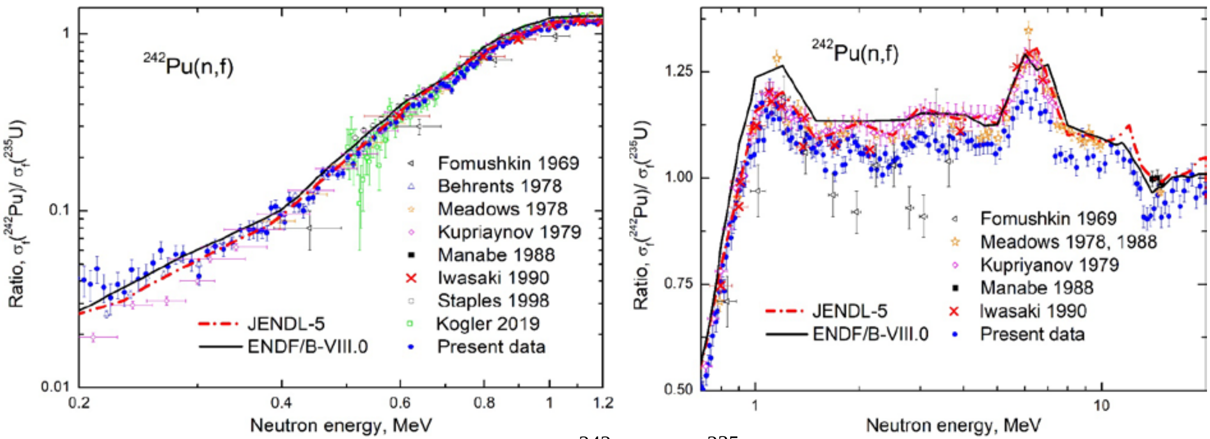

Fig. 8. Ratio of the fission cross sections of ^{242}Pu and ^{235}U in the neutron energy range from 0.2 MeV to 1.2 MeV (left) [15−19, 21−23] and from 0.7 MeV to 20 MeV (right) [18−23].

right Fig. 8. One can see that JENDL-5 evaluation follows strictly through results of Kupriyanov et al. [21].

The neutron-induced fission cross section of ^{242}Pu obtained as the product of the measured ratio R and the $\sigma_f(^{235}U)$ – existing standard of the ^{235}U(n,f) [24, 25] is presented in Fig. 9 with the data of other experiments of various types [26−34]. For example: in works [27] and [28] are used the method of accompanying particles; in [29] - measurement of the ratio of the cross section of ^{242}Pu to the cross section of ^{235}U; in [30] – measurement of the ratio of the cross section of ^{242}Pu to the cross section of ^{239}Pu; in [32] – measurement was performed relative to n-p scattering; in [33] – measurement was performed relative ^{237}Np(n,f), ^{238}U(n,f) and ^{235}U(n,f); in [34] – measurement was performed relative to n-p scattering and relative to ^{238}U(n,f). One can see that ENDF/B-VIII.0 evaluation follows Weigmann et al. data [29]. Our data are in reasonable agreement with result [30].

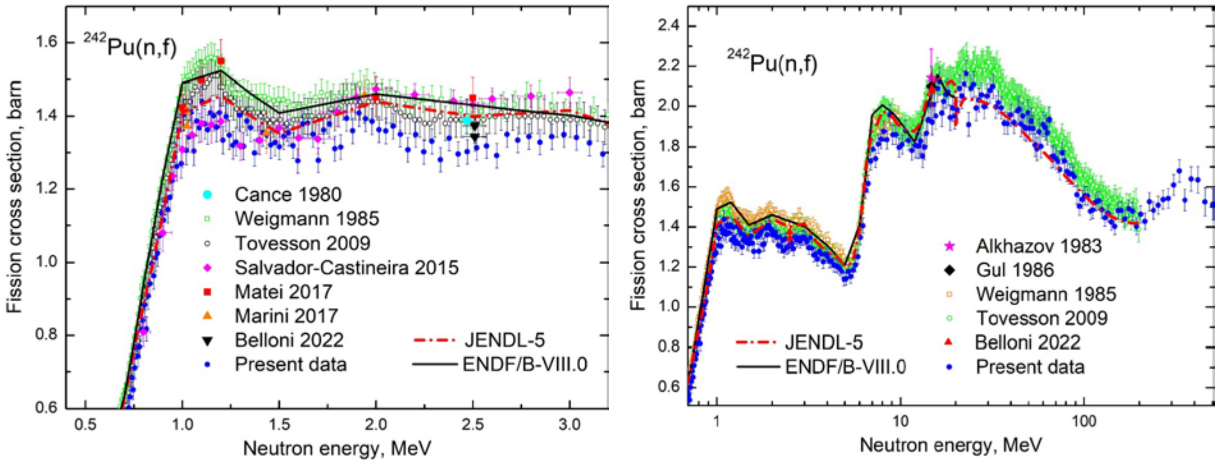

Fig. 9. Fission cross sections of ^{242}Pu obtained in this work and from other experiments (total errors are shown). The solid and dashed line consist of the estimates from the ENDF/B-VIII.0 and JENDL-5 library

Conclusion

In this work the fission cross section of ^{242}Pu is determined by the ratio method using ^{235}U as a reference. The measurements were carried out on the neutron TOF-spectrometer GNEIS at Petersburg Nuclear Physics Institute of National Research Centre «Kurchatov Institute» in the neutron energy range up to 500 MeV. The neutron induced fission cross section of ^{242}Pu was obtained in a wide energy range with the experimental uncertainty 3−4%. The shape of the fission cross section energy dependence obtained in this work is mostly consistent with the results of all earlier data obtained in TOF experiments. The differences between all existing TOF experimental data seem to be mostly related to uncertainties in the detection efficiency of the fission fragment detectors used, the neutron flux, and the target masses. The shapes of the fission cross section energy dependence in discrete energies accelerator measurements are different. This can be attributed to systematical errors of a different nature. The angular distributions of ^{242}Pu fission fragments were measured in the energy range 0.2−500 MэВ, and above 8 MeV they were measured for the first time.

Acknowledgments

The authors would like to thank the staff of the Accelerator Department of the NRC KI - PNPI for their permanent friendly assistance and smooth operation on the SC-1000 synchrocyclotron during the experiment, as well as L.S. Falev for help in creating the experimental setup.

References

1. Nuclear Science/WPEC-26, Report NEA No. 6410, OECD-NEA, 2008.
2. N.K. Abrosimov, G.Z. Borukhovich, A.B. Laptev, V.V. Marchenkov, G.A. Petrov, O.A. Shcherbakov, Yu.V. Tuboltsev, V.I. Yurchenko. Nucl. Instrum. Methods Phys. Res. A **242**, 121 (1985).
3. O.A. Shcherbakov, A.S. Vorobyev, E.M. Ivanov. Phys. Part. Nucl. **49**, 81 (2018).
4. A.S. Vorobyev, A.M. Gagarski, O.A. Shcherbakov, L.A. Vaishnene, A.L. Barabanov. JETP Letters **102**(**4**), 203 (2015).
5. A.S. Vorobyev, A.M. Gagarski, O.A. Shcherbakov, L.A. Vaishnene, A.L. Barabanov. JETP Letters **104**(**6**), 365 (2016).
6. A.S. Vorobyev, A.M. Gagarski, O.A. Shcherbakov, L.A. Vaishnene, A.L. Barabanov. JETP Letters **107**(9), 521 (2018).
7. A.M. Gagarski, A.S. Vorobyev, O.A. Shcherbakov, L.A. Vaishnene. In: "XXIII International Seminar on Interaction of Neutrons with Nuclei", Dubna, May 25-29, 2015. JINR, E3-2016-12, 2016, p.73.
8. A.M. Gagarski, A.S. Vorobyev, O.A. Shcherbakov, L.A. Vaishnene. In: "XXIV International Seminar on Interaction of Neutrons with Nuclei", Dubna, May 24-27, 2016. JINR, E3-2017-8, 2017, p.343.
9. A.S. Vorobyev, A.M. Gagarski, O.A. Shcherbakov, L.A. Vaishnene, A.L. Barabanov. In: "XXIV International Seminar on Interaction of Neutrons with Nuclei", Dubna, May 24-27, 2016. JINR, E3-2017-8, 2017, p.413.
10. A.M. Gagarski, A.S. Vorobyev, O.A. Shcherbakov, L.A. Vaishnene, A.L. Barabanov. In: "XXV International Seminar on Interaction of Neutrons with Nuclei", Dubna, May 22-26, 2017. JINR, E3-2018-12, 2018, p.342.
11. A.S. Vorobyev, A.M. Gagarski, O.A. Shcherbakov, L.A. Vaishnene, A.L. Barabanov. Proc. of the Int. Conf. "Nuclear data for Science and Technology ND-2016", September 11-16, 2016, Bruges, Belgium. EPJ Web of Conferences **146**, 04011 (2017).
12. A.S. Vorobyev, A.M. Gagarski, O.A. Shcherbakov, L.A. Vaishnene, A.L. Barabanov. JETP Letters **110**(**4**), 242 (2019).
13. J.E. Simmons, R.B. Perkins, and R.L. Henkel, Phys. Rev. **137**, B 809 (1965). EXFOR 13712004.
14. D.L. Shpak, Sov. J. Nucl. Phys. **52**, 419 (1990). EXFOR 41098002.
15. J.W. Behrens, R.S. Newbury, J.W. Magana, Nuc. Sci. Eng. **66**, 433 (1978). EXFOR 10597003.
16. P. Staples, K. Morley, Nucl. Sci. Eng. **129**, 149 (1998). EXFOR 13801004.
17. T. Koegler, A.R. Junghans, R. Beyer et al. Phys. Rev. **C 99**, 024604 (2019). EXFOR 23469002.
18. E.F. Fomushkin, E.K. Gutnikova, Sov. J. Nucl. Phys. **10**, 529 (1970). EXFOR 40012009.
19. J.W. Meadows, Nucl. Sci. Eng. **68**, 360 (1978). EXFOR 10734003.
20. J.W. Meadows, Ann. Nucl. Energy **15**, 421 (1988).
21. V.M. Kupriyanov, B.I. Fursov, B.K. Maslennikov, V.M. Surin, G.N. Smirenkin, Atomnaya Energiya, 46, 35 (1979). EXFOR 40509003.
22. F. Manabe, K. Kanda, T. Iwasaki, H. Terayama, Y. Karino, M. Baba, N. Hirakawa, Fac. of Engineering, Tohoku Univ. Tech. Report, Vol. 52, Issue. 2, p. 97 (1988). EXFOR 22282008.

23. T. Iwasaki, F. Manabe, M. Baba, S. Matsuyama, H. Kimiyama, N. Hirakawa, J. Nucl. Sci. Techn. **27**, 885 (1990). EXFOR 22211003.
24. A.D. Carlson, V.G. Pronyaev, R. Capote et al., Nuclear Data Sheets **148**, 143 (2018).
25. B. Marcinkevicius, S. Simakov, V. Pronyaev, IAEA Report No. INDC(NDS)-0681 (2015).
26. M. Cance, G. Grenier, Conf. on Nucl. Data for Sci. and Technol., Antwerp 1982, p.51 (1982). EXFOR 21821004.
27. I.D. Alkhazov, E.A. Ganza, L.V. Drapchinskiy et al, Soviet Atomic Energy **55**, 656 (1983). EXFOR 40911008.
28. K. Gul, M. Ahmad, M. Anwar & S. M. Saleem, Nuc. Sci. Eng. **94**, 42 (1986). EXFOR 31711004.
29. H. Weigmann, J.A. Wartena, C.Burkholz, Nucl. Phys. **A438**, 333 (1985). EXFOR 21931002.
30. F. Tovesson, T.S. Hill, M. Mocko, J.D. Baker, C.A. Mcgrath, Phys. Rev. C. **79**, 014613 (2009). EXFOR 14223003.
31. C. Matei, F. Belloni, J. Heyse, A.J.M. Plompen, D.J. Thomas, Phys. Rev. C. **95**, 024606 (2017). EXFOR 23334002.
32. P.Marini, L.Mathieu, M.Aiche et al., Phys. Rev. C. **96**, 054604 (2017). EXFOR 23391002.
33. P. Salvador-Castineira, T. Brys, R. Eykens et al., Phys. Rev. C. **92**, 044606 (2015). EXFOR 23280005.
34. F. Belloni, R. Eykens, J. Heyse et al., Eur. Phys. J. A **58**, 227 (2022). EXFOR 23653003.